Microwave Radiometric Technique to Retrieve Vapor, Liquid and Ice: Part II–Joint Studies of Radiometer and Radar in Winter Clouds

J. Vivekanandan, Li Li, Leung Tsang, *Fellow, IEEE,* and Chi Chan

Abstract—A neural network-based retrieval technique is developed to infer vapor, liquid. and ice columns using two- and three-channel microwave radiometers. Neural network-based inverse scattering methods are capable of merging various data streams in order to retrieve microphysical properties of clouds and precipitation. The method is calibrated using National Oceanic and Atmospheric Administration (NOAA) results in a cloud-free condition. The performance of two- and three-channel neural network-based techniques is verified by independent NOAA estimates. The estimates of vapor and liquid agree with NOAA values. In the presence of ice, the liquid estimates deviated from NOAA's estimates. One of the major contributions of the three-channel radiometer is the estimation of ice in a winter cloud. The three-channel radiometer not only improves estimates of vapor and liquid, but also retrieves the ice column. Passive remote sensing can be ameliorated with the help of active remote sensing methods. The three-channel radiometer is used for estimating columnar contents of vapor, liquid, and ice in a cloud. It is shown that vertical profiles of median size diameter, number concentration, liquid water content, and ice water content can be inferred by combining radar reflectivity and radiometer observations. The combined remote sensor method is applied to Winter Icing and Storms Project (WISP) data to obtain detailed microphysical properties of clouds and precipitation. We also derived $Z-$ Ice Water Content (IWC) and $Z-$ Liquid Water Content (LWC) relationships and they are consistent with the earlier results.

I. INTRODUCTION

THE COMBINED radar and radiometer method reduces uncertainty in cloud microphysics retrieval. An active instrument such as a pulse Doppler radar measures the range-dependent backscatter signature; however, a radiometer being a passive instrument senses the range cumulative scattering and emission characteristics. Earlier research efforts made use of both airborne and ground-based instruments [1]–[2]. In this paper, we use a ground-based three-channel radiometer and Ka-band radar for retrieving microphysical properties of clouds.

One of the important applications of the combined remote sensor method is monitoring icing situations in and around the terminal area. Icing is defined as the accretion of super-cooled liquid water (SLW) on aircraft surfaces. Especially in winter weather situations, icing continues to be one of the primary causes of aviation accidents [3]. The problem of icing detection is that of estimating SLW and mean droplet size in environments favorable to icing. Supercooled liquid water forms during the lifting of an air parcel where the ambient air temperature is below 0 °C. Confidence in detection and estimation of SLW is augmented by including the studies of other intimately related quantities such as vapor and ice.

In Part I of this paper [4], neural network-based two- and three-channel radiometer methods for retrieving vapor, liquid and ice are presented. The technique primarily uses ground-based two-channel (20.6 GHz and 31.65 GHz) or three channel (20.6 GHz, 31.65 GHz and 90 GHz) radiometer brightness temperatures. In the process of developing the neural network-based inversion model, we performed a detailed sensitivity study of brightness temperatures with respect to thirteen different atmospheric variables; namely, effective near-ground temperature (T_A), lapse rate (Γ), vapor column (V), vapor scale height (H_v), surface pressure P_0, liquid water path (LWP), liquid cloud base height (H_b), liquid cloud thickness (D), ice water path (IWP), ice cloud base height $(H_{b\text{ice}})$, ice cloud thickness (D_{ice}), mean ice particle bulk density (ρ), and ice particle radius (r_c). Based on the sensitivity study, it was found that V, LWP, and IWP were more sensitive to the three-channel brightness temperatures. A neural network-based inversion technique was used for retrieving V, LWP, and IWP from the three-channel radiometer observations. The performance of the neural network inversion model was evaluated using a simulated data set. The results showed that the neural network-based three-channel radiometer technique is capable of retrieving V, LWP, and IWP simultaneously.

In this paper, we show the practical applicability of the inversion technique using actual field measurements. A brief description of the winter field experiment and the instruments used therein is described in Section II. As described in Part I of this paper, the inversion model was constructed using the training data sets obtained from a parameterized radiative transfer model which considers profiles of temperature and humidity, in addition to scattering and emission by ice and water particles. Theoretical modeling of absorption due to a vapor continuum is not completely understood. Hence, there is a need for calibration of the neural network model because it was based only on model calculations. Since the National

Oceanic and Atmospheric Administration (NOAA) radiometer field measurements are well-calibrated and also retrievals of vapor and liquid in the absence of ice layer have been validated, we used NOAA's observations for calibrating the neural network model. The calibration procedure is described in Section III.

NOAA's technique uses only the two-channel observations for vapor and liquid retrievals. In the case of three-channel measurements, it was shown that atmospheric emission or attenuation from any of the two channels can predict that of the third channel [5]. But no attempt was made to infer any additional parameter such as IWP. Also, a comparative study between two-channel and three-channel retrieval techniques has not been performed. In Section IV, the two-channel and three-channel retrievals are compared against NOAA's results under cloudy conditions.

One of the major contributions of a three-channel radiometer is the estimation of IWP. Combining IWP with a radar-observed reflectivity profile, it is feasible to estimate ice microphysics; namely, ice water content, and average size and number concentration of the ice particles. The combined radar and radiometer method makes use of an empirical relationship between average bulk density of ice particles and reflectivity. Section V describes the combined radar and radiometer method. The combined method is used to infer liquid water content and median water drop size in a freezing drizzle situation. We performed a joint analysis of radar and radiometer measurements to demonstrate the practical applicability of the combined remote sensing method. The analysis results are presented in Section VI. Finally, the paper ends with discussion and conclusions in Section VII.

II. RADIOMETER AND RADAR INSTRUMENTATION DURING WISP

The Winter Icing and Storms Project (WISP) was conducted near Denver, CO. The scientific objectives of the project were: a) to develop and test methods using existing technology for remote detection of supercooled water, and b) to understand the formation and sustainment of regions of super-cooled water in winter storms [6]. A number of observational facilities such as radar, radiometer, radiosonde and research aircraft were deployed. A NOAA three-channel radiometer was located at Erie, CO, and it measured the brightness temperatures (T_B) at 20, 30, and 90 GHz. A NOAA two-channel radiometer was located at Plateville, CO, and it recorded T_Bs at 20 and 30 GHz. Operational characteristics of the radiometers are listed in Table I. The two and three-channel radiometers were separated by 30 km.

During WISP94, the NOAA Ka-band radar was co-located with the three-channel radiometer at Erie, CO. This radar is one of the most sensitive and can typically detect -30 dBZ echo at a 10 km range. Thus, the radar can detect clouds containing appreciable amounts of SLW in close ranges. Operational characteristics of the radar are listed in Table II. The National Center for Atmospheric Research (NCAR) launched the Cross-chain Loran Atmospheric Sounding System (CLASS). The sondes provided temperature, dew point

TABLE I
NOAA/ETL STEERABLE RADIOMETER CHARACTERISTICS

Frequencies/wavelength	20.6 GHz/ 1.46 cm
	31.65 GHz/ 0.95 cm
	90.0 GHz / 0.33 cm
Antenna beamwidth	4.0° (Dual-channel)
	2.5° (Three-channel)
Scanning modes	fixed elevation and azimuth
	fixed elevation
	fixed azimuth (min. 7.5° elevation)
Scanning rate	$0.5°\ S^{-1}$
Radiometric sensitivity (for 2-min integration time)	$0.05\ K$, rms
Estimated absolute radiometric accuracy	$0.75\ K$
Parameters measured	integrated water vapor
	integrated liquid water

temperature, pressure and wind profiles. We used the sonde measurements closest in time and space for comparing the respective radiometer observations. The data from two different field programs; namely WISP91 [7] and WISP94 [8] were analyzed.

III. RETRIEVAL OF METEOROLOGICAL PARAMETERS BY NEURAL NETWORKS

We developed retrieval methods using a neural network for two and three-channel radiometer observations in Part I of this paper. It was shown that the iterative neural network technique is capable of inferring vapor, liquid, and ice using a simulated data set. In this section, we apply the neural network method to measurements which were taken during WISP. To assure the accuracy of estimated quantities, neural network models must be calibrated. Since NOAA's technique is proven in a cloud-free condition, we used their results to calibrate the models. We analyzed data collected on two different days. We compared the results obtained using two- and three-channel measurements to show the advantage of a 90 GHz channel when ice was present.

A. Calibration of Neural Network Models

Dual-channel radiometers obtain integrated water vapor and liquid water paths by measuring brightness temperatures at 20.6 and 31.65 GHz channels. The NOAA method uses a statistical retrieval algorithm to quantify vapor and liquid from radiometer measurements [9]. It is desirable to see if neural network-based methods can produce results comparable to statistical techniques. However, both the statistical model and the neural network model have inherent bias. As discussed in Part I, uncertainty in calculation of vapor absorption introduces the bias. Using long-term observational data and theoretical

TABLE II
NOAA Ka-Band Radar Characteristics

System Gain	43.75
Polarization	H/V, Circular
Scan Rate (deg/s)	0 - 30
Beam width (deg)	0.5
Wavelength (cm)	0.87
Frequency (GHz)	34.76
Peak Power (kW)	98
Pulse Width (μs)	0.25
No. of Range Gates	328
Gate Spacing (m)	37.5 - 75

TABLE III
Scheme 2 and 3 Parameters

	Scheme 2	Scheme 3	
Retrieval variables	Range	Range	Unit
V	(0.4, 0.97)	(0.4, 0.97)	cm
LWP	(0.0, 800.0)	(0.0, 800.0)	g/m^2
IWP	(0.0, 000.0)	(0.0, 800.0)	g/m^2
r_e		(0.01, 0.15)	cm
P_0	(76.0, 86.0)	(76.0, 86.0)	Kpa
Fixed Variables	Fixed value	Fixed value	Unit
ρ		0.65	g/cm^3
H_b	1.5	1.5	Km
H_v	2.0	2.0	Km
T_A	-2.0	-2.0	$^\circ C$
Γ	6.0	6.0	K/Km
H_{bi}	3.5	3.5	Km
D	1.0	1.0	Km
D_i	2.0	2.0	Km

radiative transfer calculations, NOAA researchers estimated the bias in T_B measurements. For the NOAA model, the root mean square error for water vapor retrieval is 0.11 cm [10]. A CLASS radiosonde is used for *in-situ* observation of vapor. The bias between radiosonde and radiometer retrieval is 0.1 cm [11].

A parameterized radiative transfer model is used for generating training data sets for the forward neural network model. The major advantage of the parameterized radiative transfer model is that a detailed description of temperature and vapor density is specified by a finite number of parameters for the model calculations [4]. The training data were generated using the parameters listed under Scheme 2 in Table III. The range for the parameters in Table II are based on a long-time winter seasonal average at Denver.

The forward neural network model has two inputs for vapor and liquid and three output units for 20, 30, and 90 GHz T_Bs. The neural network is constructed with one hidden layer and 30 neurons. The weight vectors in the neural network are obtained using the simulated training data set. The three-channel T_Bs collected on March 22, 1994 and corresponding NOAA-based V and LWP pairs are used for calibrating the forward neural network model. It was a cloud-free day with zero cloud liquid water, and the vapor column varied between 0.4 and 0.6 cm. There are 5000 data points on this day and they are used as a 'truth' data set for the calibration procedure.

The 5000 pairs of V and LWP values obtained from the NOAA-based technique were used as input to the forward model. The forward model accordingly generated a second group of 5000 brightness temperatures for the 20, 30, and 90 GHz channels. The measured three-channel T_Bs were subtracted from the neural network-generated values and results were plotted in Fig. 1. The neural network model exhibits trend similar to that predicted by the NOAA model [9]. The plots show the distribution of biases between NOAA and neural network models. The mean and standard deviation of the biases are 1.503 K and 0.223 K at 20.6 GHz, 0.984 K and 0.135 K at 31.65 GHz, and 0.276 K and 0.389 K at 90 GHz. Since NOAA radiometers are well-calibrated at these three channels, the biases were added to the simulated training data set and the forward model training was performed again. The

resultant neural network model results were almost identical to NOAA's estimates in cloud-free conditions.

IV. Comparison Between Two and Three-Channel Radiometer Models

Ground-based three-channel radiometers have been in operation for several years. However, a comparison between two- and three-channel based retrievals is yet to be performed in cloudy conditions. The comparison is difficult to perform due to the following two reasons. First, to retrieve water vapor and liquid water only, the additional 90 GHz T_B may not be helpful unless it is well-calibrated. Second, the 90 GHz T_B is sensitive to ice cloud [12]. The additional warming introduced by ice layer scattering must be quantified to obtain an accurate estimate of vapor and liquid in a cloudy condition. The advantage of 90 GHz T_B is that it not only improves the estimates of vapor and liquid but also retrieves the ice column. A sensitivity study shows that brightness temperature is also sensitive to both bulk density and mean size of ice particles. With only three channels, the retrieval algorithm is not unique. The three-channel measurements provide only limited information on ice microphysics. Therefore, we have to use iterative inversion and retrieve more than three significant model parameters, i.e., vapor, liquid, ice and median size ice particles [4].

The three-channel neural network model has four input units, three output units, and one hidden layer with 30 neurons. The forward neural network input vector includes mean ice particle size in addition to path-integrated vapor, liquid, and ice water path. The output parameters are brightness temperature at three channels. The bulk density is fixed at $\rho = 0.65$ g/cm^3. The rest of the parameters are listed under Scheme 3 Table III.
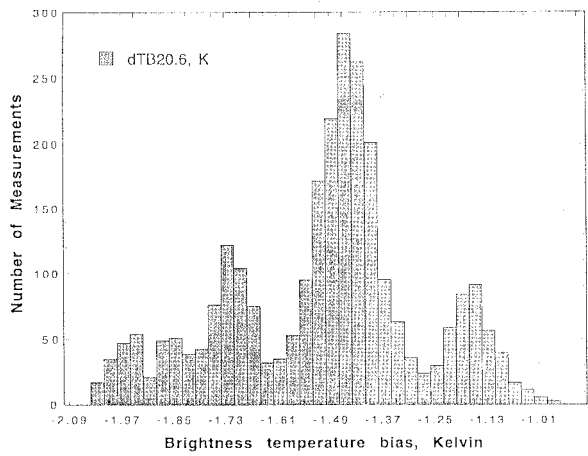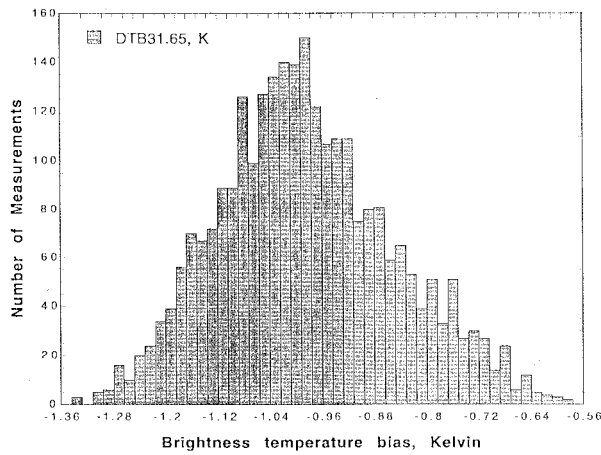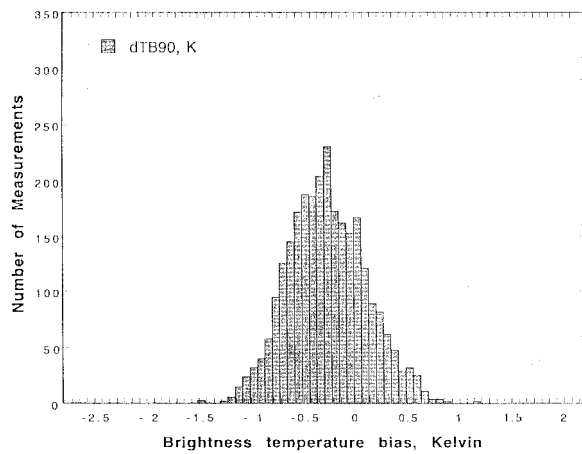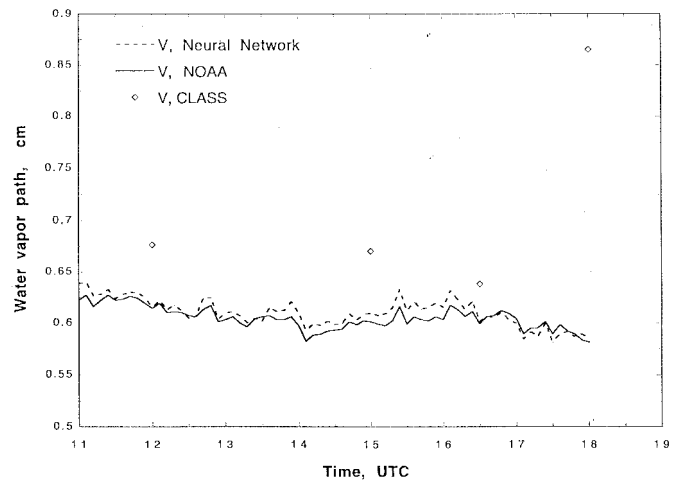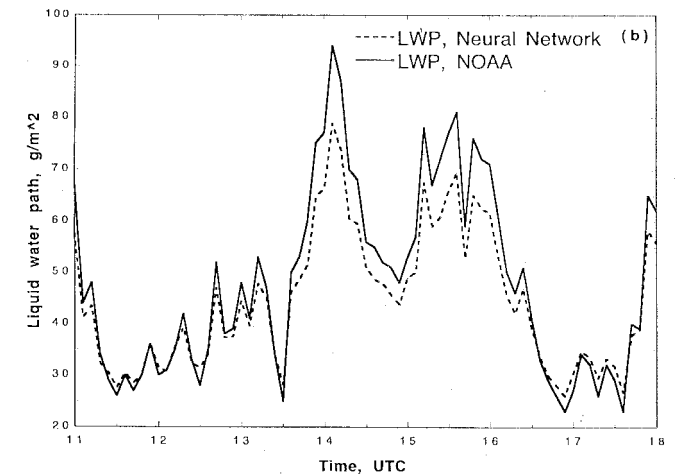
Fig. 1. Brightness temperature bias between an uncalibrated neural network model and a NOAA observation. Bias is obtained by subtracting the radiometer measurement from the neural network-based brightness temperature value: (a) 20.6 GHz, (b) 31.65 GHz, and (c) 90 GHz.

Fig. 2. Comparison of retrievals between a neural network model and a NOAA model using dual-channel radiometer measurements. Discrete data points are *in-situ* measurements of radiosonde. Radiometer data were taken on March 15, 1991 at Platteville, CO: (a) water vapor, and (b) cloud liquid water.

Before training, the simulated data were calibrated as discussed in the previous section.

The calibrated forward model provides a basis for fair comparison between inverse models. To evaluate performances of different retrieval schemes, we analyzed two- and three-channel radiometer measurements. These observations were taken on March 15, 1991. The two-channel radiometer was located at Platteville, CO, which is about 30 miles northeast of Erie. The three-channel radiometer was located at Erie. On this day, there was a persistent snowband oriented north-south in eastern Colorado, and the low clouds contained supercooled liquid water. The dynamic nature of cloud depth and its extent was monitored by the Ka-band radar. Under cloudy conditions, the spatial inhomogeneities in atmospheric quantities prevented inter-comparing measurements at Erie and Platteville.

Neural network model results for a two-channel radiometer observation are shown in Fig. 2(a). For comparison, we have also plotted the NOAA retrievals. Agreement between the NOAA and neural network-based method is quite good. During the 7 h period, vapor amounts retrieved by the neural network model almost replicate NOAA's results. Vapor is primarily characterized by the lowest frequency channel

(20 GHz). The dots indicate independent water vapor measurements by radiosondes. Fig. 2(b) shows the liquid water comparison between the two-channel neural network model. The maximum deviation of the neural network-derived liquid water path from NOAA's values is 0.015 mm and this value is within the specified accuracy of NOAA's technique. Thus the neural network-based technique is capable of duplicating the NOAA-based V and LWP retrievals.

The three-channel radiometer observations were processed using both two and three-channel neural network models and compared with NOAA's retrieval quantities. The results are shown in Fig. 3(a). The vapor estimates are almost identical in all of the methods and are not affected by scattering. The discrete dots represent the CLASS observation of vapor taken at Berthoud. The CLASS site was located 40 miles north of the radiometer location. Small differences between the CLASS observation and radiometer retrieval can be attributed to spatial inhomogeneity in vapor amounts.

Liquid retrievals are compared in Fig. 3(b). Between 1100 and 1400 UTC there is little difference. The agreement between them is better during the periods when ice is small. Since we considered scattering due to ice in radiative transfer computations, the estimated values of liquid deviate from NOAA's results in the presence of ice. According to radar observations, reflectivity value increases between 1400 and 1600 UTC suggesting the presence of an ice cloud. During this period, three-channel retrieved liquid values are the lowest and the two-channel liquid values fall in between the NOAA and the three-channel inferred quantities. As expected, NOAA's method elevated the liquid amount and neglected the presence of ice. The retrieved quantities of IWP and mean size are shown in Fig. 3(c). As suggested earlier, significant ice was present between 1400 and 1600 UTC and peaked around 1500 UTC. The mean ice particle size varies between 0.5 and 2.5 mm. There is no independent verification of IWP or mean size of ice particle. Thus, based on our simulation studies and radar observations, we are confident that a well-trained three-channel neural network is capable of inferring ice in addition to vapor and liquid.

V. RADAR AND RADIOMETER METHOD

One of the major contributions of a three-channel radiometer is the estimation of IWP. Combining IWP with a radar-observed reflectivity profile, it is feasible to estimate ice microphysics; namely, ice water content, average size, and number concentration of the ice particles. A number of combined radar and radiometer methods are proposed for investigating cloud and precipitation profiling [13]–[17]. Radar and radiometer models were developed for generating a self-consistent reflectivity and brightness temperature observation. Self-consistency between active and passive measurements improves the confidence in retrievals. In principle, the profile-based technique takes into account microphysical structure better than the regression-based techniques. In a profile-based approach, in addition to IWC and LWC, the vertical distribution of number concentration and average size of the hydrometeors are inferred. The combined radar and radiometer
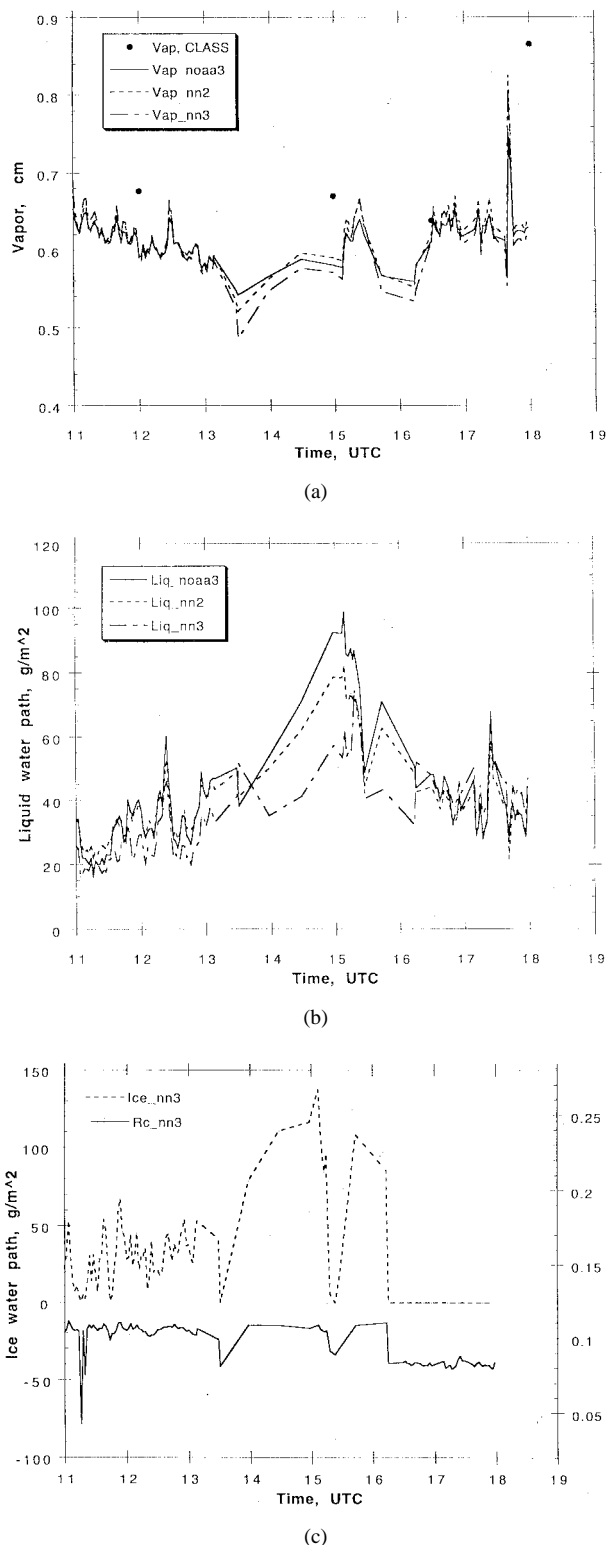

Fig. 3. Comparison of retrievals between a neural network model and a NOAA model using three-channel radiometer measurements. Discrete data points are in-situ measurements of radiosonde. Radiometer data were taken on March 15, 1991 at Erie, CO: (a) water vapor, (b) cloud liquid water, and (c) ice water path and mode radius.

method is capable of handling multilayer precipitation structures. Winter clouds are shallow, larger in spatial extent and smaller in optical depth compared to a typical thunderstorm or tropical rain clouds. In this section, we briefly discuss

inverse scattering techniques using radar. Then we describe a combined radar and radiometer method to profile liquid and ice microphysics.

A. Radar Reflectivity for IWC and LWC

For model computations, an ice particle size spectrum is usually described by the Gamma size distribution [18] as

$$N(D) = N_0 D^m \exp[-(3.672 + m)D/D_0] \ \sharp/\text{m}^3\text{mm}^{-1} \quad (1)$$

where D is the equivolume particle diameter of the ice particle, D_0 the median diameter in mm, and N_0 is in units of $\sharp/\text{m}^3\text{mm}^{-1-m}$. Scattering properties of small ice crystals and water drops can be modeled using a Rayleigh scattering approximation [19]. Using a Rayleigh scattering approximation; relationship between reflectivity (Z) and ice water content (IWC) is given as [20],

$$Z = 0.242 N_0^{-\frac{3}{4+m}} \Gamma(7+m)\rho^{(0.736+0.934m)/(4+m)}$$
$$\times \left[\frac{6000}{\pi\Gamma(4+m)} \right]^{\frac{7+m}{4+m}} (\text{IWC})^{\frac{7+m}{4+m}} \quad (2)$$

where ρ is the average ice bulk density in gcm^{-3} and $\Gamma(\cdot)$ the Gamma function. In the above equation, Z is in mm^{6}m^{-3} and ice water content (IWC) is in gm^{-3}. Ice water content is defined as

$$\text{IWC} = \frac{\pi}{6000}\rho \int D^3 N(D)dD$$
$$= \frac{\pi}{6000}\frac{\Gamma(m+4)}{(m+3.672)^{m+4}}\rho D_0^{m+4} N_0. \quad (3)$$

In a sparse media such as the atmosphere, radar reflectivity is proportional to IWC and total number concentration ($N_t \ \sharp/\text{m}^3$) for a given m and D_0 [21]. The N_t is obtained by integrating the size distribution as

$$N_t = \int N(D)dD = N_0 \frac{\Gamma(m+1)}{(m+3.672)^{m+1}} D_0^{m+1}. \quad (4)$$

Using the above three equations, the following relationships are derived:

$$\text{IWC} = \frac{\pi}{6000}\frac{\Gamma(m+4)}{\Gamma(m+1)}(m+3.672)^{-3}\rho D_0^3 N_t \quad (5)$$

$$Z = 0.242\frac{\Gamma(m+7)}{\Gamma(m+1)}(m+3.672)^{-6}\rho^{1.934} D_0^6 N_t \quad (6)$$

or

$$Z = \frac{1452}{\pi}\frac{\Gamma(m+7)}{\Gamma(m+4)}(m+3.672)^{-3}\rho^{0.934} D_0^3(\text{IWC}). \quad (7)$$

The above equations offer an interesting insight into the Z and IWC relationship. For a fixed ρ and m, the parameters Z and IWC are proportional to $D_0^6 N_t$ and $D_0^3 N_t$, respectively. This indicates that D_0^3 introduces a major source of ambiguity in the linear relationship between IWC and Z. For a given reflectivity, there is more than one IWC value as a function of D_0 and N_t along the contours $D_0^6 N_t = $ constant. In other words, we can search IWC iteratively on a $D_0^6 N_t$ line toward a desired value while keeping the Z unchanged. Fig. 4 shows the contours of Z and IWC on a $D_0 - N_t$ plane. The following
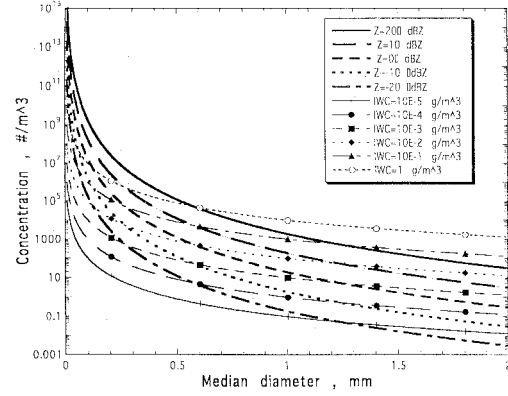

Fig. 4. Isopleths of radar reflectivity and ice water content on the plane of particle concentration (N_t) and median diameter (D_0).

empirical rule is used to specify the average bulk density in generating Fig. 4:

- $\rho = 0.90$ if $Z \leq -5$ dBZ
- $\rho = 0.60$ if $-5 < Z \leq 0$ dBZ
- $\rho = 0.20$ if $0 < Z \leq 10$ dBZ
- $\rho = 0.01$ if $Z > 10$ dBZ.

There are two reasons for using the above empirical rule. Generally, the bulk density of an ice particle reduces as the size increases for a specified mass of a particle [20]. Second, our goal is to investigate possible ways of combining radar with radiometer; this empirical rule is an approximation and can be modified later by incorporating precise microphysical information depending on winter storm types.

The main advantage of the combined radar and radiometer method is that it facilitates a procedure for constructing a self-consistent microphysical profile $[N_t(z), D_0(z), \rho(z)]$ for a given set of brightness temperature and radar reflectivity observations. The inferred microphysical profile would

1) reproduce the observed reflectivity profile,
2) constrain the IWP which is specified by radiometer retrieval, and
3) satisfy constraints imposed by cloud physics such as typical number concentration, and median size.

It should be noted that imposing constraints is actually a way of incorporating additional information and rules into the combined retrieval algorithm. In this paper, we only force the ice particle size and concentration to be in a reasonable range: 0.05 mm $\leq D_0 \leq 3.00$ mm and $0 \leq N_t \leq 2 \times 10^5$ m^{-3}[22].

As discussed earlier, we use an iterative approach to obtain the microphysical profile using radar and radiometer observations. Since the number of unknowns in microphysical profiles is larger than what can be handled by a limited set of measurements, the inversion procedure is ill-posed. As an ill-posed problem, the profiling technique depends on initial estimates of size distribution parameters of the particular precipitation and cloud. For the cases studied here, we chose a constant D_0 profile as an initial estimate. It implies that the variation in radar reflectivity is mainly due to changes in ice particle concentration, rather than due to the median diameter. Taking the radiometer retrieved ice water path IWP$_\text{radiom}$ as an upper limit on the total ice column in the cloud, the initial

value of median diameter $(D_{0-\text{initial}})$ can be found from

$$\begin{aligned}\text{IWP}_{\text{radiom}} &= \sum(\text{IWC})\Delta z \\ &= 2.186 \times 10^{-3}(m+3.672)^3 \frac{\Gamma(m+4)}{\Gamma(m+7)} D_{0-\text{initial}}^{-3} \\ &\quad \cdot \left(\sum \rho^{-0.934\,76} Z \Delta z\right). \quad (8)\end{aligned}$$

Based on this initial guess of D_0, we can distribute the radiometer-derived IWP in proportion to the Z profile measured by radar. The iterative approach is built using (5)–(7) to find an ice water content profile which gives an IWP as close as possible to $\text{IWP}_{\text{radiom}}$.

In the above case, we only discussed ice clouds. A similar set of equations can be obtained for liquid clouds,

$$\text{LWC} = \frac{\pi}{6000} \frac{\Gamma(m+4)}{\Gamma(m+1)}(m+3.672)^{-3} D_0^3 N_t \quad (9)$$

$$Z = \frac{\Gamma(m+7)}{\Gamma(m+1)}(m+3.672)^{-6} D_0^6 N_t \quad (10)$$

and

$$Z = \frac{6000}{\pi} \frac{\Gamma(m+7)}{\Gamma(m+4)}(m+3.672)^{-3} D_0^3(\text{LWC}) \quad (11)$$

where $0 \le D_0 \le 100\ \mu\text{m}$, and $0 \le N_t \le 1000/\text{cm}^3$ for clouds over land. A typical freezing rain which forms by collision and coalescence processes produces a liquid cloud.

VI. OBSERVATIONS

The above-described measurement techniques using radar and radiometer sensors are applied to the actual data. We report on observations in winter storms made with the three-channel radiometer and Ka-band radar. The characteristics of these instruments are listed in Tables I and II. As outlined in an earlier section, the model makes use of a number of assumptions which are applicable to winter storm situations. The inferred value of vapor and liquid is compared with NOAA's results. However, there is no independent measurement of IWP except for theoretical simulation studies performed in Part I. *In-situ* observations of research aircraft provide only limited information on ice microphysics, and also the sampling volumes of radar and aircraft differ widely. Hence, no attempt was made to compare it with aircraft observations. In the following sections, we demonstrate the utility of the combined remote sensor method. We first present a day-long measurement from a multilayer cloud which went through various stages of evolution. Primarily, the cloud contained ice and vapor and the amount of liquid is small. The second example shows a freezing drizzle case with no ice.

A. Measurements from February 8, 1994

On February 8, 1994, a cold surge from the north went by Denver and the surface temperature dropped from 0.6 °C to −8.3 °C within an hour. Once the surge went through the area, it stalled on the Palmer Divide, which is south of Erie. The weather system produced light snow over the observational area. Very little snow accumulation was noted and the cloud contained little liquid. By 1800 UTC most of the light snow
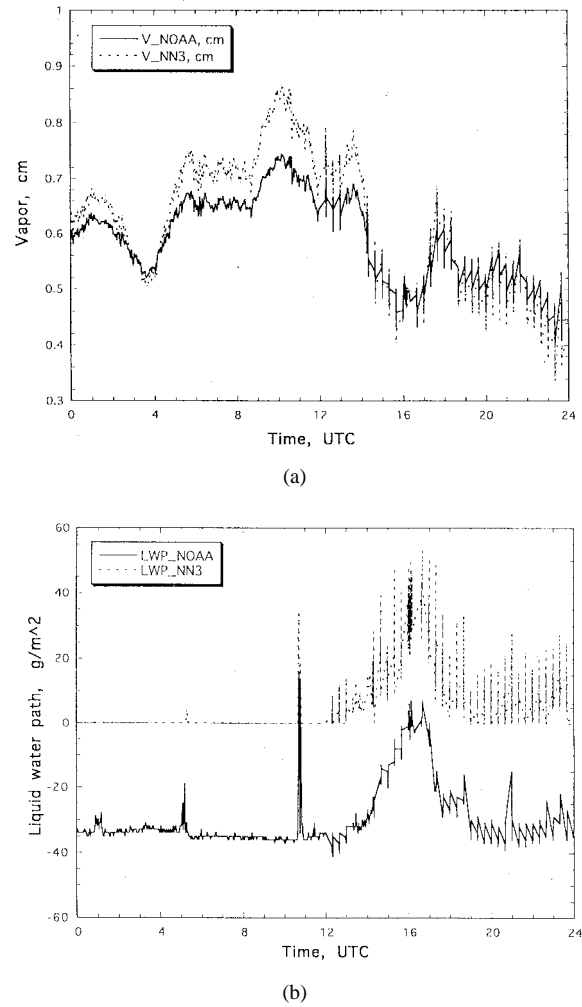

(a)

(b)

Fig. 5. Comparison of retrievals between a neural network model and a NOAA model using the three-channel radiometer measurements: (a) water vapor and (b) cloud liquid water. Radiometer data were taken on February 8, 1994 at Erie, CO.

dissipated and the clouds became thin with low reflectivity values.

The radiometer collected data throughout the day. We processed the radiometer measurements to obtain water vapor, cloud liquid and ice using a three-channel neural network model. To avoid the scan angle dependence on T_B observations, we used only the zenith pointing data. The gaps in the plot correspond to scanning radiometer data and are joined by straight lines. Fig. 5(a) shows the time series of vapor and follows NOAA's estimate. The period between 0500 and 1400 UTC corresponds to elevated vapor amounts. The ice particles grew primarily through a vapor deposition process in these clouds. Fig. 5(b) shows the plot of the total liquid column. Except for the bias, the trend in the liquid matches NOAA's values. The error margin for integrated liquid is 0.05 mm for the NOAA three-channel retrieval [23]. The NOAA-based liquid values are smaller than the error margin and hence no liquid was detected by the NOAA technique. During this period, the Ka-band reflectivity increased from −15 dBZ to 10 dBZ and also multi-layer cloud structures were formed. Even though there was no *in-situ* verification of liquid, we
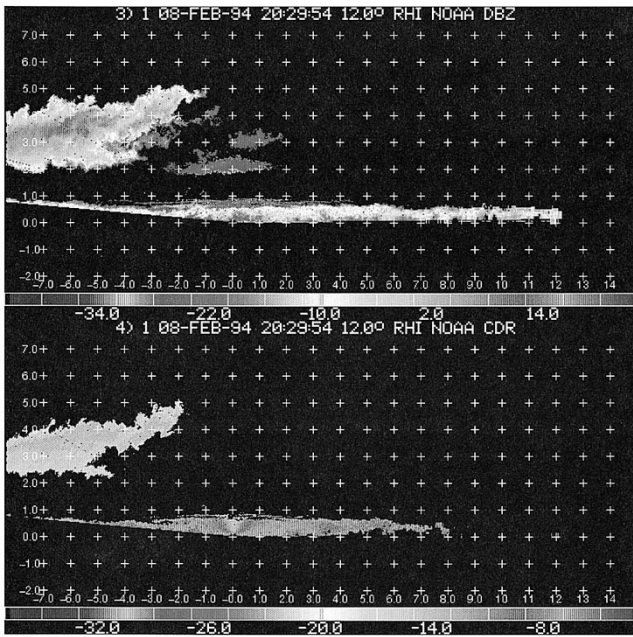
Fig. 6. Radar reflectivity and circular depolarization ratio on February 8, 1994 at 2029 UTC. The range height indicator plot is displayed with 1 km grid overlay. The positive range is along 12° azimuth, negative range is along 192° azimuth and the radar is at the origin. The cloud has a multilayer structure and has three layers right above the radar.

are confident that cloud liquid was present between 1300 and 1700 UTC. The amount of liquid is small; nevertheless, the neural network method is able to retrieve the liquid.

The Ka-band radar was in operation between 1300 and 2300 UTC. The radar collected RHI scans for every 30 min. Thus, we have simultaneous observations of radiometer and radar along the zenith for every 30 min. Fig. 6 shows RHI images of reflectivity and circular depolarization ratio (CDR) taken at 2029 UTC. The cloud has three different layers and they are discontinuous. The layer closest to the ground contains ice particles predominantly and the presence of ice is also confirmed by cross-polarization (circular depolarization ratio) radar measurement. The two upper-layer reflectivities are considerably lower and this is consistent with the small amount of liquid inferred using a radiometer [see Fig. 5(b)]. Hence, it is highly probable that the upper-layer consists of small supercooled liquid drops. The lack of any depolarization signatures from this layer might be due to liquid drops or a weak depolarization signal.

We used the combined radar and radiometer method to infer median size (D_0) and total number concentration in cloud using the method described earlier. The plots of estimated IWP and average median size are plotted in Fig. 7. The radar and radiometer estimates of IWP show reasonable agreement and their trends agree well. The differences between them might be attributed to some of the assumptions in the model such as bulk density of ice particle and size distribution. It should be noted that these initial results can be improved by tuning some of the assumptions and incorporating additional observations. The value of D_0 varies between 0.1 and 2.4 mm. As discussed earlier, the parameter D_0 is one of the major factors which introduces ambiguity in radar estimates of IWC and hence the
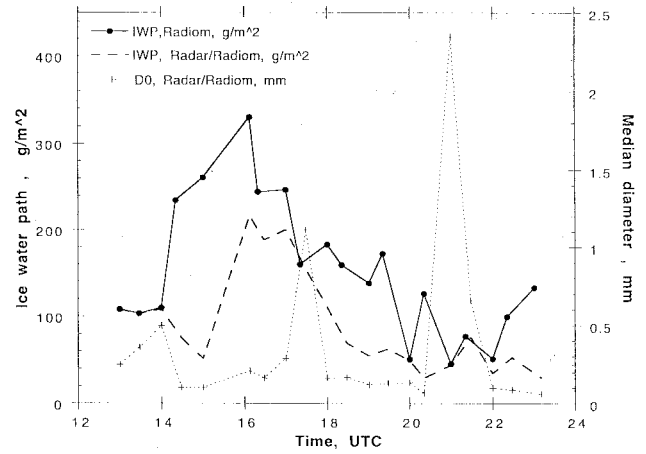

Fig. 7. Ice water path and median diameter retrievals from a three-channel radiometer and a combined radar and radiometer method.
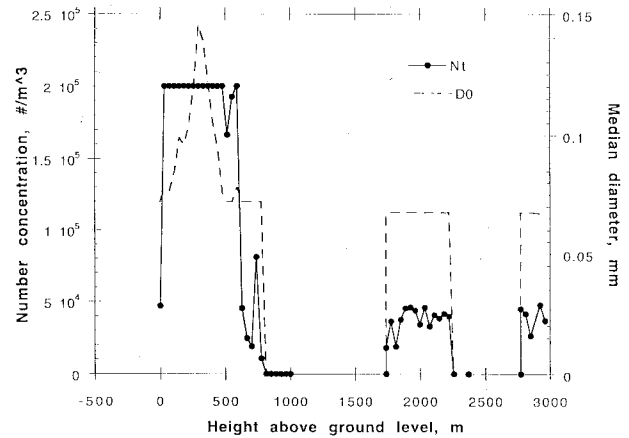

Fig. 8. An example of retrieved profiles of water and ice particle concentration and median diameter.

proposed combined method has the potential for reducing the uncertainty in IWC estimates. A vertical microphysics profile derived using the combined methods is shown in Fig. 8. The maximum D_0 in the ice layer is 140 μm and the upper liquid layer contains liquid drops with D_0 values around 70 μm. The concentrations of ice and liquid particles are also shown.

Using radiometer-based IWP estimates, we showed earlier the possibility of estimating IWC as a function of radar reflectivity. Typically, the relationship between reflectivity and IWC is expressed in a power law or in a linear equation as

$$Z(\text{dBZ}) = C_1 + C_2 \log(\text{IWC}) \tag{12}$$

where C_1 is the intercept and C_2 is the slope. Depending on the mathematical formulation the slope can be either $10\frac{m+7}{m+4}$ or 10 [see (2) and (7)]. In the method outlined earlier, we obtained D_0, hence for a specified ρ, the Z vs IWC equation should exhibit a slope of 10. But in practice, there are natural variations in size distribution and bulk density which lead to a slope which is neither 10 or $10\frac{m+7}{m+4}$. The fitted equation using several Z and IWC couplets from a number of
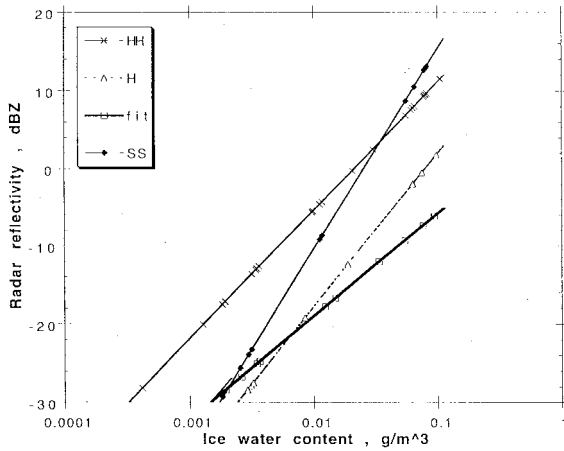
Fig. 9. Empirical relationship between radar reflectivity and ice water content from several vertical profiles of microphysics on February 8, 1994 by a combined radar/radiometer method. Other published empirical relationships ([27]) are presented for comparison.

winter storms is plotted in Fig. 9. The equation has a slope of 13.19 and it is comparable to the previously published results. The form of these equations depends on the amount of averaging over the respective microphysical regime. Hence any improvement in the $Z - \mathrm{IWC}$ relation should come from improved microphysical information, such as bulk density, N_0, and D_0 as shown in (2) and (7). It is to be noted that the previously published empirical $Z - \mathrm{IWC}$ relationship is based on forward problems: calculations of radar reflectivities from known size distribution spectra [24]. In this paper, the regression ($Z - \mathrm{IWC}$) relationship is based on an inverse problem: retrievals of size distribution spectrum parameters using radar and radiometer methods.

B. Measurements from February 7, 1994

In Section V we outlined a method of inferring cloud liquid microphysical properties using a combined radar and radiometer method. It is relatively easier to analyze freezing drizzle than an ice cloud for the following reasons: a) the retrieval of a liquid water path using a radiometer is a well-established technique and the retrieval accuracy is widely accepted, and b) liquid cloud droplets are small in size and spherical in shape and Rayleigh approximation always holds in the frequencies of our interest.

On February 7, 1994, NOAA's Ka-band radar and radiometer observed a layer of liquid between 1149 and 1600 UTC. Fig. 10 shows an example of radar measurement taken around 1149 UTC. The cloud was shallow and reflectivities were less than -20 dBZ. The absence of a depolarization signature and cloud liquid water observed by the radiometer confirm that no ice was present in the cloud. The liquid drops were formed by a collision and coalescence process. It was a freezing drizzle situation. The combined radar and radiometer method is used to retrieve N_t and average D_0 values. Radar and radiometer data were analyzed for a 4 h duration and the results are shown in Fig. 11. Radar-based estimates of LWP are in agreement with radiometer values. The median diameter of cloud drops varies between 10 and 60
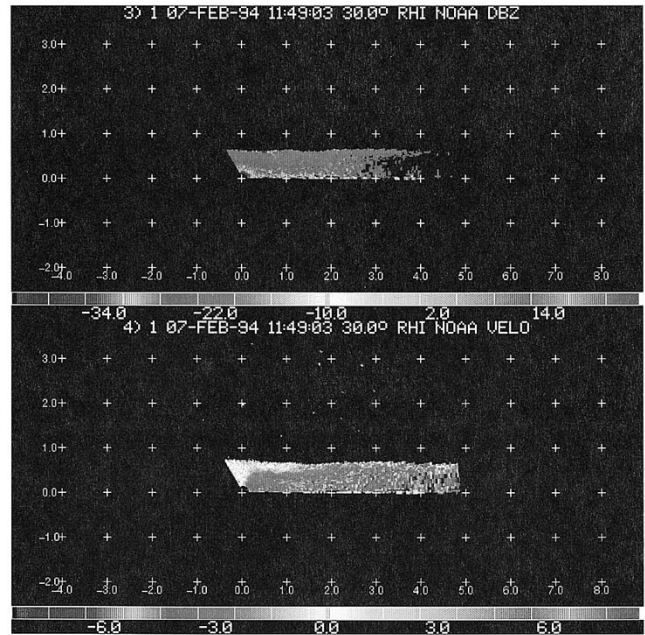

Fig. 10. Radar observations of reflectivity and radial velocity on February 7, 1994 at 1149 UTC. The range height indicator plot is displayed with 1 km grid overlay.
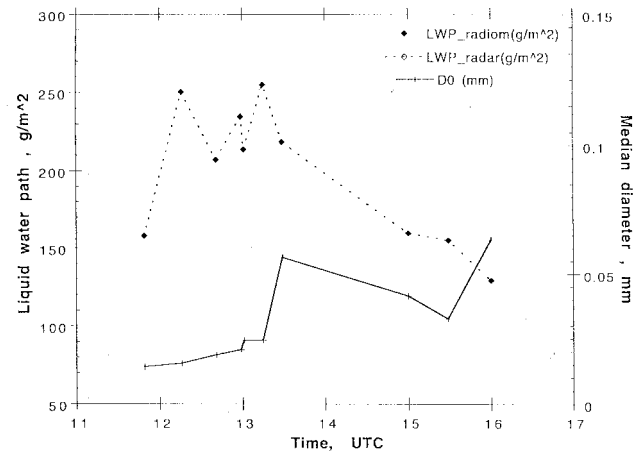

Fig. 11. Liquid water path and median diameter retrievals from a radiometer and a combined radar and radiometer method.

microns. This is different from the ice cloud case where IWP retrievals showed differences (see Fig. 7). We also obtained the $Z - \mathrm{LWC}$ regression equation for freezing drizzle. We selected four radar reflectivity and microphysics profiles at 1149-1216-1259-1309 UTC, and plotted a $Z - \mathrm{LWC}$ scatter plot as shown in Fig. 12. The regression line of this scatter plot is $Z = -16.89 + 11.214 \log(\mathrm{LWC})$. For comparison, the $Z - \mathrm{LWC}$ relationships from Atlas [25] and Sauvageot *et al.* [26] are also presented in Fig. 12. Once again, the regression line is in general agreement.

VII. CONCLUSION

We demonstrated practical applicability of a neural network-based inversion technique to estimate vapor, liquid and ice. We considered scattering due to ice in radiative transfer
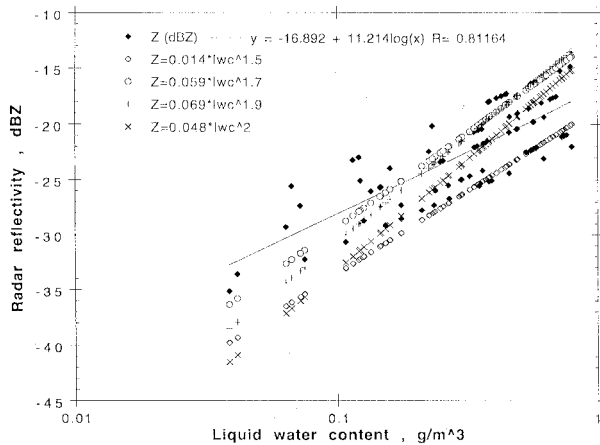
Fig. 12. Empirical relationship between radar reflectivity and liquid water content from several vertical profiles of microphysics on February 7, 1994 by a combined radar and radiometer method. Other published relationships are presented for comparison.

computations in conjunction with an accurate emission model. The measurements collected during WISP were analyzed. The inverse models were calibrated using NOAA's results in a cloud-free condition. We compared the results obtained using two and three-channel observations. In a cloud-free condition, neural network-based results agreed with NOAA's estimates. Also, the agreement between NOAA's results and neural network model-based estimates is good in the absence of ice layers. Estimates of cloud liquid water deviated from NOAA's results in the presence of ice. In addition to vapor and liquid, the three-channel method estimated IWP and mean ice particle size. However, there is no independent verification of ice microphysics.

This novel technique provides physical insight into the radiative transfer process and can be used to enhance our understanding of existing radiometer algorithms. Most importantly, this approach does not depend on *in situ* measurements. In other words, a radiosonde database is not required to develop an inverse model. Therefore, this method is very economical and it can be designed in a short time frame for a specified climatic region.

We also proposed a combined radar and radiometer method. We examined the $Z - \text{IWC}$ relationships on a $N_t - D_0$ plane and identified D_0^3 as an important source of ambiguity in an empirical $Z - \text{IWC}$ relationship. Retrievals of integrated ice water and liquid water content from radiometers are distributed according to radar measurements. These profiles are then used as an initial estimate and are adjusted iteratively to obtain microphysics profiles which are consistent with radar measurements. The estimated values of mean ice particle size and cloud droplet size are typical for a winter cloud. The variations in $Z - \text{LWC}$ and $Z - \text{IWC}$ relationships due to averaging over cloud microphysics were also discussed. Experimentally-derived $Z - \text{LWC}$ and $Z - \text{IWC}$ relationships are consistent with other published studies.

Although we dealt with a ground-based radiometer and radar in this work, it is straightforward to apply this method to airborne and spaceborne platforms as in the case of TOGA

COARE and TRMM [28] projects, respectively. These projects are designed for combined radar and radiometer remote sensing of precipitation systems. Compared with other existing models, this novel approach emphasizes physical modeling and integration of different measurements. In other words, this method offers a technique for combining physical inverse models with climatological statistics, surface meteorological observations, and cloud microphysics.

REFERENCES

[1] J. Vivekanandan, J. Turk, and V. N. Bringi, "Comparison of precipitation measurements by the advanced microwave precipitation radiometer and multiparameter radar," *IEEE Trans. Geosci. Remote Sensing*, vol. 31, pp. 860–870, 1993.
[2] M. K. Politovich, B. B. Stankov, and B. E. Martner, "Determination of liquid water altitudes using combined remote sensors," *J. Appl. Meteorol.*, vol. 34, no. 9, pp. 2060–2075, 1995.
[3] M. K. Politovich, "Aircraft icing caused by large supercooled droplets," *J. Climate Appl. Meteorol.*, vol. 28, no. 9, pp. 856–868, 1989.
[4] L. Li, J. Vivekanandan, C. H. Chan, and L. Tsang, "Microwave radiometer techniques to retrieve vapor, liquid and ice: Part I—Development of neural network-based inversion method," this issue, pp. 224–236.
[5] E. R. Westwater, J. B. Snyder, and M. J. Falls, "Ground-based radiometer observations of atmospheric emission and attenuation at 20.6, 31.65 and 90 GHz: A comparison of measurement and theory," *IEEE Trans. Antennas Propagat.*, vol. 38, pp. 1569–1580, Oct. 1990.
[6] R. M. Rasmuseen, M. K. Politovich, J. Marwitz, W. Sand, J. McGinely, J. Smart, R. Pielke, S. Rutledge, D. Wesley, G. Stossmeister, B. Stankov, and D. Burrows, "Winter icing and stroms project," *Bull. Amer. Meteorol. Soc.*, vol. 73, no. 7, pp. 951–974, 1992.
[7] R. Rasmussen and M. Politovich, *Winter Icing and Storms Project (WISP): Scientific Overview*, National Center for Atmospheric Research rep., June 1990.
[8] G. Stossmeister, *Winter Icing and Storms Project 1994: Operations Plan*, National Center for Atmospheric Research rep., Feb. 1994.
[9] E. R. Westwater, "Ground-based microwave remote sensing of meteorological variables," *Atmospheric Remote Sensing by Microwave Radiometry*, M. A. Janssen, Ed. New York: Wiley, 1993, ch. 4.
[10] B. E. Martner, D. B. Wuertz, B. B. Stankov, R. G. Strauch, E. R. Westwater, K. S. Gage, W. L. Ecklund, C. L. Martin, and W. F. Dabberdt, "An evaluation of wind profiler, RASS and microwave radiometer performances," *Bull. Ameri. Meteorol. Soc.*, vol. 74, no. 4, pp. 599–613, 1993.
[11] S. F. Clifford, J. C. Kaimal, R. J. Lataitis, and R. G. Strauch, "Ground-based remote profiling in atmospheric studies: An overview," *Proc. IEEE*, vol. 82, pp. 313–355, Mar. 1994.
[12] J. Vivekanandan, J. Turk, and V. N. Bringi, "Ice water path estimation and characterization using passive microwave radiometry," *J. Appl. Meteorol.*, vol. 30, pp. 1407–1421, 1991.
[13] R. Meneghini and K. Nakamura, "Range profiling of the rain rate by airborne weather radar," *Remote Sens. Environ.*, vol. 31, pp. 193–209, 1990.
[14] R. Meneghini, J. R. Wang, H. Kumagai, and T. Ighuchi, "Description of a radar/radiometer method and its application to airborne measurements over stratiform rain," *IGARSS'94*, JPL, Pasadena, CA, 1994, pp. 1773–1775.
[15] T. Kozu, K. Nakamura, R. Meneghini, and W. C. Boncyk, "Dual-parameter radar rainfall measurement from space: A test result from an aircraft experiment," *IEEE Trans. Geosci. Remote Sensing*, vol. 29, pp. 690–703, 1991.

[16] M. Marzoug and P. Amayenc, "Improved range profiling algorithms of rainfall rate from a spaceborne radar with path-integrated attenuation constraint," *IEEE Trans. Geosci. Remote Sensing*, vol. 29, pp. 584–592, 1991.

[17] B. B. Stankov, B. E. Martner, and M. K. Politovich, "Moisture profiling of the cloudy winter atmosphere using combined remote sensors," to be published.

[18] C. W. Ulbrich, "Natural variations in the analytical form of the raindrop size distribution," *J. Climate Appl. Meteorol.*, vol. 22, pp. 1764–1775, 1983.

[19] R. Doviak, J. Dusan, and S. Zrnic, *Doppler Radar and Weather Observations*, 2nd ed.   New York: Academic, 1993.

[20] J. Vivekanandan, V. N. Bringi, M. Hagen, and P. Meishner, "Polarimetric radar studies of atmospheric ice particles," *IEEE Trans. Geosci. Remote Sensing*, vol. 32, pp. 1–10, Jan. 1994.

[21] L. Tsang, J. Kong, and R. Shin, *Theory of Microwave Remote Sensing*. New York: Wiley, 1985, p. 613.

[22] P. V. Hobbs and A. L. Rango, "Ice particle concentration in clouds," *J. Atmos. Sci.*, vol. 42, pp. 2523–2549, 1985.

[23] Personal communication with NOAA Environmental Technology Laboratory, June 1994.

[24] S. Y. Matrosov, "Radar reflectivity in snowfall," *IEEE Trans. Geosci. Remote Sensing*, vol. 31, pp. 451–461, 1992.

[25] D. Atlas, "The estimation of cloud parameters by radar," *J. Meteorol.*, vol. 11, pp. 309–317, 1954.

[26] H. Sauvageot and J. Omar, "Radar reflectivity of cumulus," *J. Atmos. Ocean. Tech.*, vol. 4, pp. 264–272, 1987.

[27] A. J. Heymsfield and A. G. Palmer, "Relationships for deriving thunderstorm anvil ice mass for CCOPE storm water budget estimates," *J. Clim. Appl. Meteorol.*, vol. 25, pp. 691–702, 1986.

[28] J. Simpson, R. F. Adler, and G. North, "A proposed tropical rainfall measuring mission (TRMM) satellite," *Bull. Amer. Meteorol. Soc.*, vol. 69, pp. 278–295, 1988.

J. Vivekanandan, for a photograph and biography, see this issue, p. 236.

Li Li, photograph and biography not available at the time of publication.

Leung Tsang, (S'73–M'75–SM'85–F'90) for a biography, see this issue, p. 236.

Chi Chan, photograph and biography not available at the time of publication.